

Computational Modeling of Axonal Microtubule Bundles under Tension

Stephen J. Peter^{†‡} and Mohammad R. K. Mofrad^{†*}

Molecular Cell Biomechanics Laboratory, Departments of [†]Bioengineering and [‡]Mechanical Engineering, University of California, Berkeley, California

ABSTRACT Microtubule bundles cross-linked by tau protein serve a variety of neurological functions including maintaining mechanical integrity of the axon, promoting axonal growth, and facilitating cargo transport. It has been observed that axonal damage in traumatic brain injury leads to bundle disorientation, loss of axonal viability, and cognitive impairment. This study investigates the initial mechanical response of axonal microtubule bundles under uniaxial tension using a discrete bead-spring representation. Mechanisms of failure due to traumatic stretch loading and their impact on the mechanical response and stability are also characterized. This study indicates that cross-linked axonal microtubule bundles in tension display stiffening behavior similar to a power-law relationship from nonaffine network deformations. Stretching of cross-links and microtubule bending were the primary deformation modes at low stresses. Microtubule stretch was negligible up to tensile stresses of ~1 MPa. Bundle failure occurred by failure of cross-links leading to pull-out of microtubules and loss of bundle integrity. This may explain the elongation, undulation, and delayed elasticity of axons following traumatic stretch loading. More extensively cross-linked bundles withstood higher tensile stresses before failing. The bundle mechanical behavior uncovered by these computational techniques should guide future experiments on stretch-injured axons.

INTRODUCTION

Microtubule bundles cross-linked by microtubule-associated protein (MAP) tau are a major structural feature of the axon, an elongated projection that conducts electrical impulses away from the body of a neuron. These microtubule bundles are located in the interior portion of the axon, and alongside neurofilaments and a thin actin cortex form the axonal cytoskeleton. A variety of neurological functions are mediated by these bundles, including maintaining mechanical integrity and shape of the axon, promoting axonal growth, and facilitating cargo transport (1,2). The morphology of axonal microtubule bundles cross-linked by tau protein are in fact the main feature that distinguishes axons from dendrites, another elongated neuronal projection, as shown in Fig. 1. Axonal microtubule bundles typically contain a density of microtubules of ~10–200 microtubules/ μm^2 , yielding ~10–100 microtubules in a typical cross section (3). It has been found that the average length of these microtubules is ~4 μm in the axon of cultured rat hippocampal neurons (4). Bundled microtubules are arranged in polarized arrays (5), allowing for directed fast transport of cargo such as amyloid precursor protein along the axon via molecular motors attached to the microtubules. Impaired transport of cargo such as amyloid precursor protein can lead to focal accumulation in the axoplasm, resulting in axonal swelling and beading (6).

In axons, microtubules are coated with MAP tau, a natively unfolded filamentous protein abundant in the central nervous system. The most common MAP present

in the axon is MAP tau, the protein responsible for the cross-linked structure of the axonal microtubule bundle (see Fig. 1). Tau proteins have a typical molecular mass between 50 and 75 kDa depending on the specific isoform (7). Through complimentary dimerization with other tau proteins, bridges are formed to nearby microtubules to create bundles (8,9). These bundles formed by tau protein in the axon have a typical edge-to-edge spacing of ~20 nm and are generally hexagonally packed (10).

Traumatic axonal injury is a characteristic feature of focal and diffuse traumatic brain injury, characterized by local disorientation of the axonal microtubule bundle, beading of the axon, impaired axonal transport, retraction of the synapse, and axonal degeneration (11–14). Traumatic axonal injury has been studied through a number of in vitro studies in which axons are subjected to traumatic stretch injury. A recent study shows evidence of microtubule rupture in the vicinity of axonal beads formed due to traumatic stretch injury (15). Microtubules have been shown to rupture at strains of ~50% (16). It is also possible that the cross-links formed by tau proteins are failing under traumatic loading, leading to loss of the bundled architecture.

The lateral reinforcement of microtubules by cross-linking to the cytoskeleton has been shown to enhance their ability to bear compressive loads (17). Though microtubules are conventionally regarded as bearing compressive loads, in certain circumstances such as in traumatic stretch injury, they are placed in tension. Experimental techniques have yet to characterize the immediate mechanical behavior of axonal microtubule bundles in tension. Computational modeling techniques have been employed to investigate the mechanical behavior of the filaments comprising the cytoskeleton (18,19) and have been used to investigate

Submitted June 11, 2011, and accepted for publication November 22, 2011.

*Correspondence: mofrad@berkeley.edu and <http://biomechanics.berkeley.edu>

Editor: Andrew McCulloch.

© 2012 by the Biophysical Society
0006-3495/12/02/0749/9 \$2.00

doi: 10.1016/j.bpj.2011.11.4024

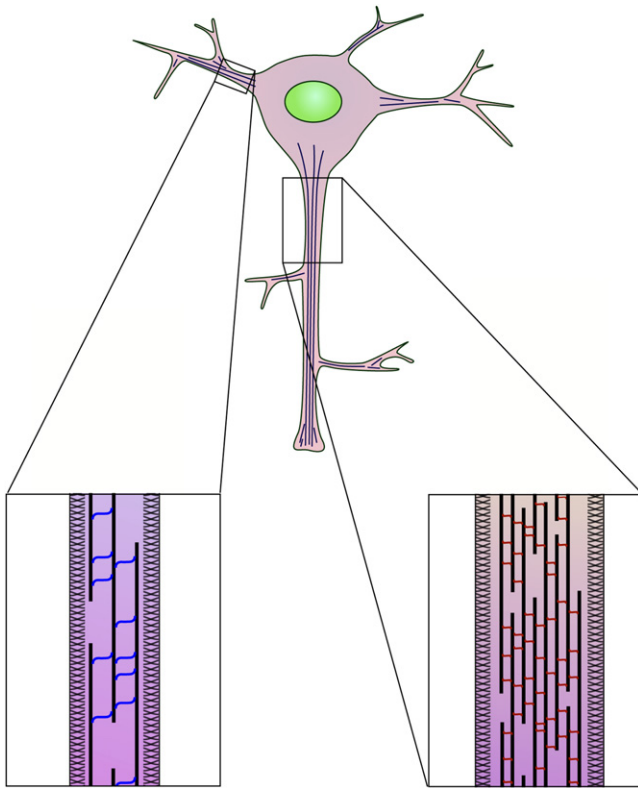


FIGURE 1 Schematic of a neuron with an axon and dendrites. Microtubules, represented by thick, black lines, are bundled by MAP proteins. Bundle morphology is dependent on the bundling MAP. Right inset: Axon showing microtubules cross-linked by tau protein (*red*). Left inset: Dendrite showing microtubules cross-linked by MAP2 (*blue*). (Not drawn to scale).

cross-linked networks (20–22). These studies have emphasized the importance of the cross-link properties and network/bundle geometry in the overall mechanical behavior. Nonaffine behavior of cytoskeletal networks has been characterized previously, whereby realignment of network fibers leads to stiffening at high stresses (23,24). A few studies have investigated the mechanics of cross-linked square microtubule bundles. Tolomeo et al. (25) used theoretical and computational modeling to show that the shear resistance provided by the cross-links greatly increases microtubule bundle bending stiffness. Furthermore, a theoretical investigation by Bathe et al. (26) has characterized distinct bundle bending stiffness regimes resulting from the competition between filament stretching and cross-link shearing. This study seeks to characterize the mechanical behavior of axonal microtubule bundles in tension. The model emphasizes relevance to axonal microtubule bundles in tension by including hexagonal bundle architecture, discontinuous microtubules, material parameter prediction based on experimental data, and failure behavior. It is proposed that axonal microtubule bundles exhibit nonlinear mechanical behavior in tension due to nonaffine network deformations. Furthermore, it is suggested that the mechan-

ical behavior of MAP tau is critical to the bundle tensile response, and that MAP tau may fail under traumatic stretch loading.

MATERIALS AND METHODS

Discrete element formulation

Discrete bead-spring models are often employed to model the mechanical behavior of filaments and filamentous networks (20,27–29). In such models, point masses interact via potentials representing various phenomena such as elasticity, damping, and steric repulsion. A bead-spring model of the axonal microtubule bundle allows for sufficient size and complexity of the system with only modest computational demands. This type of model also allows for the investigation of irregular, physiologically accurate geometries; this is especially difficult in theoretical mechanics studies. Previous studies have focused on bundles with continuous filaments spanning the entire bundle length; this neglects the impact of discontinuities on the mechanical properties of the bundles, which in all likelihood significantly decreases bundle stiffness, a consideration this study seeks to investigate. Discontinuities in microtubules can easily be incorporated and the role of a variety of geometric and mechanical parameters can be investigated. As a result of these considerations, a model of axonal microtubule bundles can be developed that closely replicates physiological bundles and has sufficient spatial and temporal detail.

Bead-spring models capture higher level deflections of the filaments, such as bending and axial deflections, using interaction potentials between beads that approximate the mechanical equations. Fig. 2 shows a schematic of the representation of bundle filaments by a network of beads connected by springs. The current model is concerned primarily with the mechanical stretching of microtubules under a moderate force regime. These forces will quickly stretch the microtubules past the entropic-dominated and into a linear mechanical stretching regime, a transition characterized previously (30). As such, a linearly elastic mechanical stretching potential was employed between microtubule beads. Filament beads were connected by linear springs with potential V_s of the form in the equation,

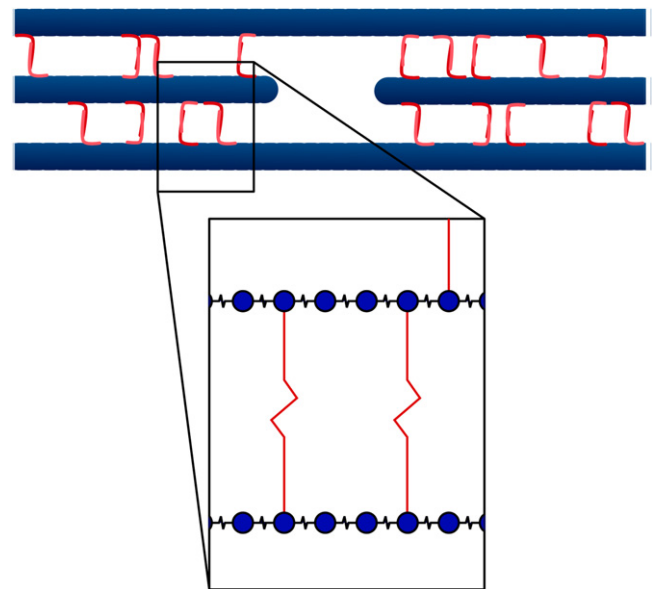


FIGURE 2 Schematic of the bundle filaments represented by a network of beads connected by spring elements. Angular springs representing bending stiffness are also included between microtubule elements (not shown). (Not drawn to scale).

$$V_s = k_s \frac{(\|\mathbf{r}\| - l_0)^2}{2}, \quad (1)$$

where k_s is the spring constant, \mathbf{r} is the separation distance, and l_0 is the unstretched length of the spring. The spring constant k_s is related to the material properties of the filament in the equation,

$$k_s = \frac{EA}{l_0}, \quad (2)$$

where E is the Young's modulus of the filament, A is the cross-sectional area of the filament, and l_0 is the unstretched bead spacing. The tau protein cross-links were modeled as two-node linear spring elements, a representation common to a number of cross-linked network models (26).

The bending potential was represented by a harmonic potential as a function of the bend angle θ . The bending potential V_b therefore took the form in the equation,

$$V_b = k_b \frac{(\theta - \theta_0)^2}{2}, \quad (3)$$

where k_b is the bending spring constant, θ is the angle between subsequent elements, and θ_0 is the rest angle of the bend. The bending spring constant is related to the material properties of the filament in the equation,

$$k_b = \frac{EI}{l_0}, \quad (4)$$

where EI is the flexural rigidity of the filament and l_0 is the unstretched bead spacing. The flexural rigidity EI of a polymer is related to its persistence length in the equation,

$$EI = l_p k_B T, \quad (5)$$

where l_p is the persistence length, k_B is the Boltzmann constant, and T is the temperature.

Steric repulsion of the beads in the system was necessary to prevent penetration of the beads on one microtubule into those of another. The potential associated with the steric repulsion in such a coarse-grained model is only meant to prevent penetration and the form is somewhat arbitrary. An exponentially decaying potential V_{SR} was used of the form shown in the equation,

$$V_{SR} = \epsilon_0 e^{-\|\mathbf{r}\|/\sigma_0}, \quad (6)$$

where ϵ_0 is the energy scaling parameter, \mathbf{r} is the distance between sterically interacting beads, and σ_0 is the steric radius. The steric radius was set to the outer microtubule radius, 12.5 nm, and the energy scaling parameter was iteratively selected to prevent penetration with minimal long-range effects. A cutoff radius of $2.4 \sigma_0$ was used to truncate the steric interaction for computational efficiency while preventing filament penetration.

Bundle geometry

Using in-house code, a hexagonal bundle of 19 rows with a center-to-center microtubule spacing of 45 nm was created, to correspond to the desired 20 nm edge-to-edge spacing. Each row consisted of $8 \mu\text{m}$ of microtubule length with one discontinuity; this created 38 separate microtubules with an average continuous microtubule length of $4 \mu\text{m}$. It was made certain that discontinuities were not placed too close to the edges of the bundle by restricting discontinuities to the central 80% of each row. An arbitrary gap length of 150 nm was used at the discontinuity in each row. A representative bundle generated using this method is shown in Fig. 3. The microtubule bead spacing was set to 10 nm to sufficiently resolve bending between

cross-links. A discretization study was performed, and elastic energy storage behavior was shown to converge at this 10 nm spacing.

Cross-links were distributed between neighboring microtubules throughout the bundle based on desired average cross-link spacing. The tau cross-link bead mass was added to the mass of beads where cross-link elements were added. The number of cross-links N_{CL} in the computational bundle was calculated to provide an average cross-links spacing δ_{CL} of 25, 50, 75, or 100 nm in the equation,

$$N_{CL} = \frac{N_{MT} L_{MT}}{\delta_{CL}}, \quad (7)$$

where N_{MT} is the number of microtubules, and L_{MT} is the average continuous microtubule length. The number of microtubules N_{MT} and average continuous microtubule length L_{MT} were 38 and $4 \mu\text{m}$, respectively.

Simulation procedure

The velocity Verlet algorithm was used to calculate bead trajectories over the duration of the simulations. The interaction force \mathbf{F}_{ji} is calculated from the interaction potential in the equation,

$$\mathbf{F}_{ji} = -\nabla V(\mathbf{r}_{ij}), \quad (8)$$

where V is the interaction potential and \mathbf{r}_{ij} is the vector from bead i to bead j . Brownian forces were not considered in the model due to the high persistence length of microtubules and dominance of mechanical stretch deformations. Brownian effects would have a much greater significance in the entropic stretch range, and should not significantly contribute to the stress-strain behavior in the mechanical stretch regime.

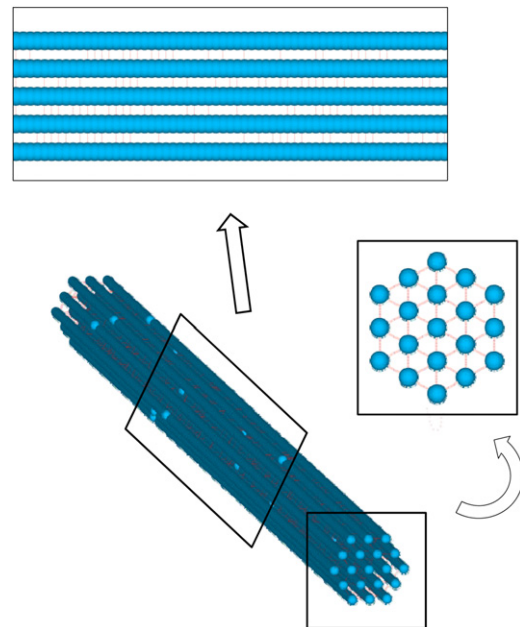


FIGURE 3 Example simulation geometry generated using in-house code. Beads are drawn with a radius of 12.5 nm to show microtubules at the correct width (the physical radii of beads are not important except in steric repulsion). Elements between microtubule beads are not shown. Bundle length is $8 \mu\text{m}$, and microtubules are placed with a 20 nm edge-to-edge spacing. Note the single randomly placed discontinuity in each row and the random distribution of cross-links at a specified average spacing (25 nm average shown).

An axial tensile stress was applied by distributing forces to the ends of the microtubules at either end of the bundle. This tensile stress is meant to represent the stress on the microtubule bundle itself and not necessarily that of the whole axon. These two quantities may not be equal based on the load sharing between all structural components of the axon. Total tensile force was first calculated by multiplying the desired tensile stress by the total cross-sectional area of the 19 microtubule ends. This force was then divided evenly among the end beads of the microtubules. The total applied force was ramped to its maximum value over the first 10% of the simulations to prevent excessive oscillations. The energy scaling parameter in Eq. 6 was set to 1×10^{-18} Nm to prevent penetration of beads in neighboring microtubules. In-house code written in FORTRAN was used to integrate the equations of motion and calculate bead trajectories. A time step of 0.1 ps was used for stability and computational efficiency. The steady-state strain values at a given tensile stress were calculated by allowing the bundle to come to rest in a dynamic simulation. A small numerical damping of bead velocities was included in simulations to prevent excessive oscillations and dissipate kinetic energy. This numerical damping allowed the bundle to come to rest when the elements carried enough elastic energy to resist the tensile stress.

In dynamic simulations of failure, a modified predictor-corrector velocity Verlet algorithm with resistance coefficients to simulate drag on elements was used. Critical strain criteria were enforced for elements; upon reaching this critical strain, elements were deleted from the simulation. For microtubule elements, the critical strain was set at 0.5 based on experimental measurements of the rupture strain (16). The critical strain of the tau cross-links was set to 1.0, corresponding approximately to the jump-out length from a study on tau dimerization by Rosenberg et al. (9). This criterion represents the length at which the tau protein dimers can no longer maintain a bridge between neighboring microtubules.

Material parameters

Experimental data from a number of studies were used to assign values to the spring constants in the harmonic potential functions represented by Eqs. 1–6. The values of the parameters used in the study are shown in Table 1 and their derivation are detailed in this section. Values were chosen to fall within the observed physiological range of axonal microtubule bundles.

Measured values of the elastic modulus of microtubules are in the range of hundreds of MPa to a few GPa. A thorough study of the anisotropic mechanics of microtubules that agreed well with experimental data was performed by Pampaloni et al. (31). A value of 1.5 GPa was used for the microtubule Young's modulus E_{MT} , which falls within the typical range of reported values and corresponds with the Pampaloni study (31). This study also predicted a length-dependent persistence length l_p of microtubules. Based on a microtubule length of $4 \mu\text{m}$, a persistence length of $420 \mu\text{m}$ was predicted. Using Eq. 5 and this persistence length, a microtubule flexural rigidity $(EI)_{MT}$ of 1.8×10^{-24} Nm² was obtained.

Studies of the mechanical properties of single dimerized tau cross-links are unavailable, so an estimate of the Young's modulus had to be obtained. By estimating a persistence length of tau dimers on the order of a micron and using Eq. 5, a Young's modulus of tau protein cross-links E_{CL} of 5.0 MPa was used. The estimation of this parameter is further complicated because the stretching mode of the cross-link is unclear; stretching of the tau filaments, the tau-tau bond, or the tau-microtubule bond are all candidates. As such, this value is decidedly approximate, but the qualitative bundle behavior should not be significantly altered unless the true modulus is incorrect by multiple orders of magnitude.

Study design

Using realistic bundle geometries created using in-house FORTRAN code, the stress-strain and failure behavior of axonal microtubule bundles were investigated. The parameter under investigation, the average cross-link spacing, was investigated at levels of 25, 50, 75, and 100 nm. These levels

TABLE 1 Material parameters used to calculate simulation parameters

Parameter	Value	Source
Microtubule Young's modulus, E_{MT}	1.5 GPa	Pampaloni et al. (30)
Microtubule persistence length, l_p^{MT}	420 μm	Pampaloni et al. (30)
Microtubule flexural rigidity, $(EI)_{MT}$	1.8×10^{-24} Nm ²	Pampaloni et al. (30)
Tau cross-link Young's modulus, E_{CL}	5.0 MPa	Estimate
Microtubule element length, l_0^{MT}	10 nm	
Tau cross-link element length, l_0^{CL}	45 nm	
Microtubule axial spring constant, k_s^{MT}	47.1 N/m	Calculated, Eq. 2
Microtubule bending spring constant, k_b^{MT}	1.8×10^{-16} Nm	Calculated, Eq. 4
Tau cross-link axial spring constant, k_s^{CL}	3.925×10^{-2} N/m	Calculated, Eq. 2
Microtubule bead mass, m_{MT}	1.48375×10^{-21} kg	
Tau cross-link bead mass, m_{CL}	2.0×10^{-22} kg	
Microtubule resistance coefficients, C_n^{MT}, C_t^{MT}	2.1191, 1.2700	
Tau cross-link resistance coefficients, C_n^{MT}, C_t^{MT}	5.9555, 4.9181	
Time step, Δt	0.1 ps	
Steric energy scaling parameter, ϵ_0	1×10^{-18} Nm	
Steric radius, σ_0	12.5 nm	

of average cross-link spacing correspond to values typical of the estimated physiological range. However, no explicit data are available regarding the average cross-link spacing in vivo. As such, the estimated range was based on images of axonal microtubule bundles cross-linked by MAP tau. This parameter study allowed for the investigation of the effects of increasing the degree of bundling, corresponding to the density of cross-link bridges on a given length of microtubule. At each level of average cross-link spacing, five computational bundles were generated by randomizing the locations of cross-links and discontinuities in each row. These five configurations allowed for statistical significance and prevented skewing the results toward a particular configuration's response. These bundles were then subjected to uniaxial stress parallel with the bundle axis at levels of 1 kPa, 10 kPa, 100 kPa, 1 MPa, and 10 MPa, and the bundle strain was calculated in each case. Failure simulations were performed with one computational bundle at each average cross-link spacing at tensile stresses from 10 to 600 MPa.

RESULTS AND DISCUSSION

Bundle steady-state stress-strain behavior

A total of 100 simulations were performed to determine the steady-state bundle stress-strain behavior at each level of cross-link spacing. The simulated bundles came to rest at a steady-state configuration within simulation durations of 2 μs . The results of these simulations are plotted in Figs. 4 and 5 (for data, see Table S1 in the Supporting Material). These simulation results clearly show strain-stiffening

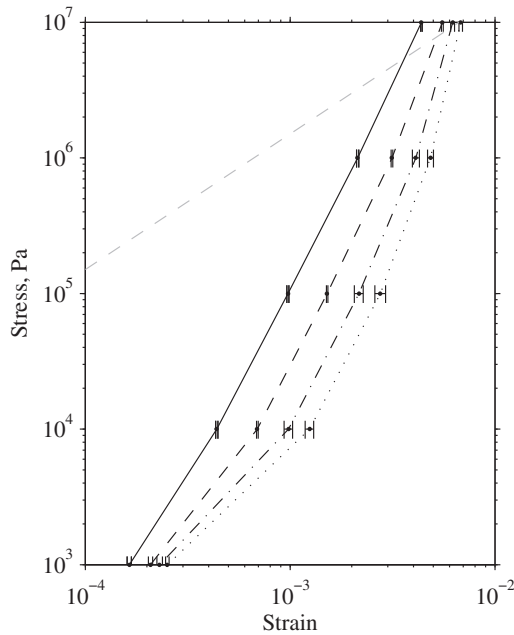


FIGURE 4 Steady-state bundle stress-strain curves in tension. Error bars representing the standard error are shown. Curves are shown for 25 nm (solid line), 50 nm (dashed line), 75 nm (dash dotted line), and 100 nm (dotted line) average cross-link spacing. The stress-strain response of continuous bundles (without discontinuities) is shown as the gray dashed line, where the entirety of the load is carried by microtubule stretching. Strain stiffening behavior of the bundle response is evident due to nonaffine network deformations.

behavior of the axonal microtubule bundles. The stress-strain behavior of the bundles with the densest distribution of cross-links, at 25 nm average spacing, is well represented ($R^2 = 0.9963$) by a power-law fit of the form in the equation,

$$\sigma = (3.65 \times 10^{13}) \epsilon^{2.82}, \quad (9)$$

where σ is the tensile stress in Pa and ϵ is the bundle strain. The cases with lower densities of cross-links are not well represented by basic power-law fits, suggesting a more complicated stress-strain relationship.

The complex stiffening behavior displayed by the bundles is especially interesting given that the spring elements are all linearly elastic. Nonaffine bundle deformations and varying load sharing between elastic storage modes are responsible for this effect. Graphs depicting the energy storage in the different elastic modes, microtubule stretch, microtubule bending, and cross-link stretch, are shown in Fig. 4 (for data, see Table S1). Energy associated with steric repulsion is not included and is only significant in the 10 MPa simulations. At small deformations, cross-links rotate leading to lateral forces on microtubules. As a result, the elastic energy is shared primarily between the cross-link stretch and microtubule bending storage modes. In fact, microtubule stretch contributes <5% of the energy storage up to a tensile stress of 1 MPa (see Table S1). It is important to note that these nonaffine deformations are a result of the microtubule discontinuities within the bundle; idealized parallel continuous rows would carry the entirety of the elastic energy in microtubule stretch at any strain level. In bundles with a higher cross-link density, cross-link stretch stores a larger portion of the elastic energy compared to microtubule bending (see Fig. 4). It was observed that at high stress, the microtubules begin to shift toward the bundle centerline and straighten out, causing the energy stored in microtubule stretch to drastically increase while the microtubule bending energy significantly decreases. Furthermore, at high stress the cross-links carry more elastic

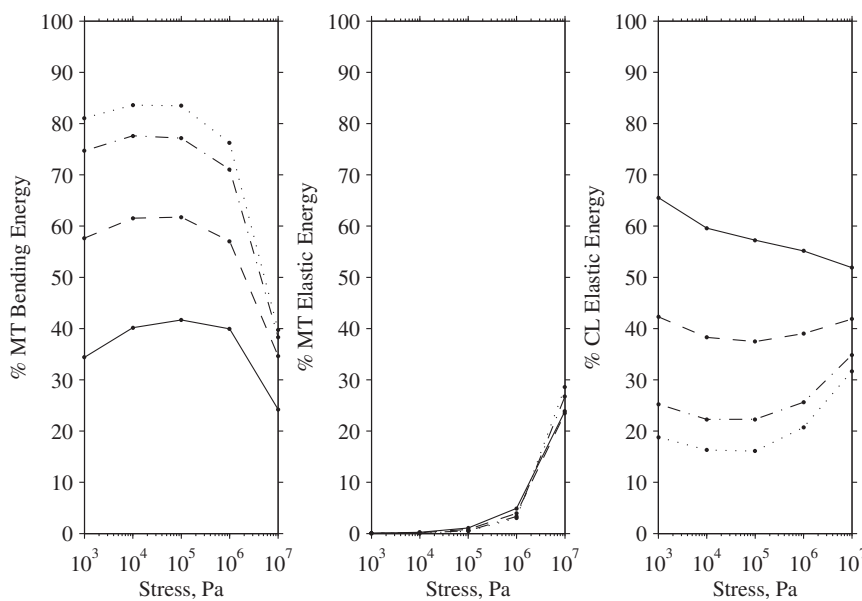


FIGURE 5 Steady-state energy sharing curves of elastic energy storage modes. Curves are shown for 25 nm (solid line), 50 nm (dashed line), 75 nm (dash dotted line), and 100 nm (dotted line) average cross-link spacing. From left to right: percentage of energy stored in microtubule bending, percentage of energy stored in microtubule stretching, percentage of energy stored in cross-link stretching. Microtubule stretching contributes <5% of the elastic energy storage up to a tensile stress of 100 kPa.

energy because they have rotated into closer alignment with the bundle axis. Steric repulsion became extremely significant in the 10 MPa simulations, indicating that the bundle had tightened near to the steric limit. Given that the formulation of the steric repulsion is not strictly physically accurate; the results of the simulations in this steric regime should be interpreted with caution. If accurate, this tightening behavior may have implications relating to in vivo bundle behavior; tau proteins on the microtubule surface have been suggested to serve as steric brushes preventing full bundle collapse and resisting microtubule sliding (32).

These results predict that axonal microtubule bundles are relatively compliant at smaller loads. In such a situation, the bundle network simply reconfigures itself with microtubules experiencing negligible mechanical stretch. At higher loads, the bundle becomes stiffer in tension to effectively resist large axonal deformations. Mechanical stretching of microtubules becomes significant and the bundle tightens toward its centerline.

Bundle dynamics and failure

Bundle response dynamics and failure were investigated to examine the acute mechanical events of stretch loading. Hydrodynamic damping was enforced by modeling elements as cylinders moving through a stationary viscous fluid. Bundles with average cross-link spacing of 25, 50, 75, and 100 nm were subjected to tensile stresses between 10 and 600 MPa. Critical strain criteria of 0.5 for microtubule

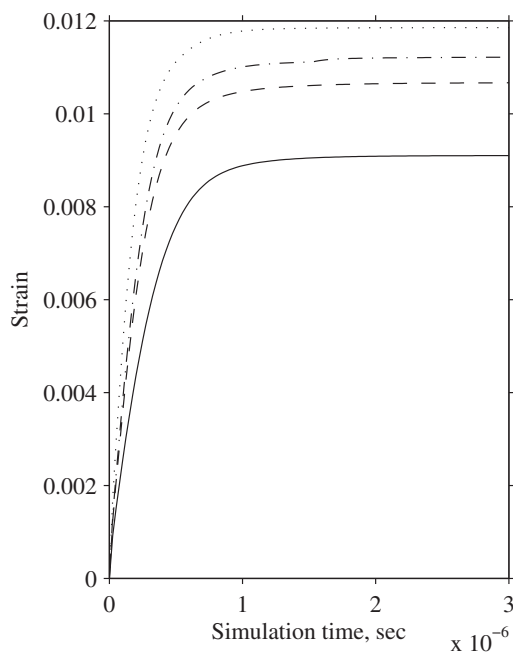


FIGURE 6 Bundle strain dynamics at 50 MPa tensile stress. Curves are shown for 25 nm (solid line), 50 nm (dashed line), 75 nm (dash dotted line), and 100 nm (dotted line) average cross-link spacing. Steady-state bundle strains are reached in 1–2 μ s.

elements and 1.0 for cross-links were enforced. Catastrophic bundle failure was characterized by the initiation of rapidly increasing element failure and bundle length. Steady-state bundle strains were reached in 1–2 μ s in simulations where failure was not evident, as shown in Fig. 6. Failure was evident at 500, 300, 200, and 200 MPa for average cross-link spacing of 25, 50, 75, and 100 nm, respectively, as shown in Fig. 7. This indicates that more extensively cross-linked bundles can withstand higher tensile stresses before failing. These simulations showed bundle failure occurring entirely by failure of the cross-links with the microtubule elements remaining intact. This mode of bundle failure, which shall be referred to as microtubule pull-out, is characterized by failure of the cross-links leading to the microtubules being pulled past one another and out of a tightly bundled configuration. Fig. 8 shows a simulated microtubule bundle undergoing pull-out due to cross-link failure. Pull-out of microtubules may explain the significant elongation of axons following traumatic stretch seen in experiments. With the failure of the cross-linked architecture and elongation of the bundle, previous studies (26) predict a reduced bundle bending stiffness. Axonal undulations observed following traumatic stretch injury are perhaps a result of these combined effects. The new distribution of the microtubules in the axon would take time to be rearranged back into a tightly bundled configuration,

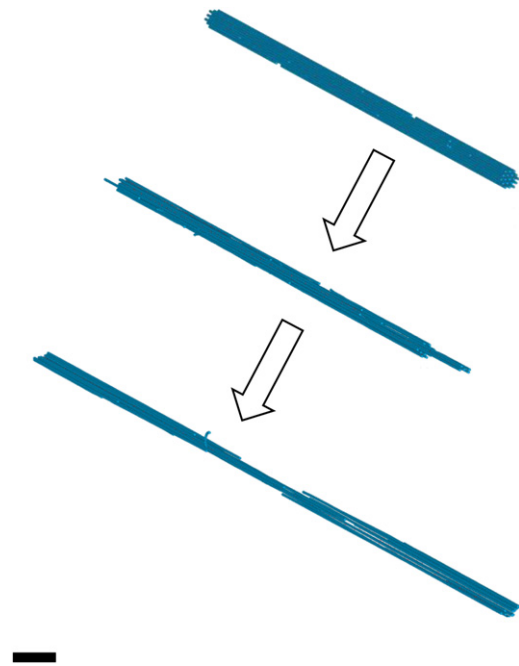


FIGURE 7 Catastrophically failing microtubule bundle showing microtubule pull-out. Average cross-link spacing is 50 nm, and the applied tensile stress is 300 MPa. Element failure was monitored, indicating only failure of cross-link elements. Tightening of the bundle toward the centerline is also evident. Simulation times are 0 μ s (top), 1.25 μ s (middle), and 5 μ s (bottom). (Scale bar = 1 μ m).

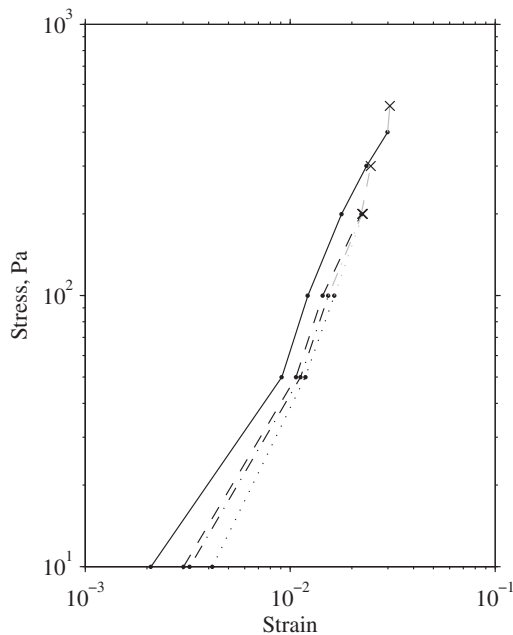


FIGURE 8 Steady-state stress-strain curves of bundles with microtubule and cross-link critical strain failure criteria enforced. Strain values at the initiation of failure are indicated by an *x*. Curves are shown for 25 nm (*solid line*), 50 nm (*dashed line*), 75 nm (*dash-dotted line*), and 100 nm (*dotted line*) average cross-link spacings. Lower cross-link densities resulted in catastrophic bundle failure at lower stress and strain values.

providing a possible explanation of the delayed elasticity of injured axons.

These observations do not explain the evidence of microtubule breakage seen in some experiments. Evidence of microtubule rupture, characterized by catastrophically depolymerizing microtubules, has been observed in the areas of axonal swellings in a study by Tang-Schomer et al. (15). Furthermore, an interesting experimental observation has been made that axons contain a range of short and long microtubules (4,33); one might suspect that different length classes of microtubules may have different mechanical responses. One would suspect longer microtubules *in vivo* are more extensively anchored (34) and less likely to experience pull-out which may lead to rupture. Additionally, the more extensive coating of tau protein on longer microtubules would lead to a higher resistance to the sliding seen in microtubule pull-out. Rupture of these long microtubules in conjunction with pull-out may explain the impaired transport leading to the formation of axonal beads, but this association would need to be investigated further.

The observations from the failure simulations lead to a general hypothesis about the primary mechanical events in the axonal microtubule bundle due to traumatic stretch injury. Under traumatic loading, tau cross-links may fail leading to microtubule pull-out where microtubules slide past one another. Longer, heavily anchored microtubules may be ruptured leading to catastrophic depolymerization.

The axonal microtubule bundle attains an elongated, structurally weakened configuration leading to acute axonal elongation, undulation, and potentially axonal beading. Cellular biochemical events may then lead to repair of the microtubule bundle or complete degeneration of the axon.

Limitations of the model

The current model has a number of limitations that should be carefully considered. Assumptions were necessary to minimize computational expenses, and led to a model best suited for tensile loading. The elements in the system, both microtubule and tau cross-link, were assumed to follow a linear elastic constitutive relationship. This assumption is less valid in an entropic stretching regime, in compressive loading, and potentially in a high force regime. Simulations were performed with no Brownian motion considered. Anchoring of the bundle to the rest of the cytoskeleton, such as the neurofilaments network and the actin cortex, was not considered. Chemical dynamics were not considered, and as such, the effects of the polymerization and depolymerization of microtubules and the formation and dissociation of cross-links were neglected. The material parameters of the microtubules are based on currently available experimental results and the elastic modulus of the cross-links is an approximation. The sensitivity of the model to relevant system parameters is detailed in Appendix A. Future work will seek to improve the accuracy of the model by relaxing some of these assumptions and considering more of the related biochemical phenomena.

CONCLUSION

The primary mechanical events in axons experiencing traumatic loading are complex and difficult to investigate experimentally. This study has demonstrated the suitability of discrete computational models in investigating the mechanical behavior of cross-linked axonal microtubule bundles under tensile loading. Simulations were performed with loads in normal physiological and traumatic ranges.

The computational bundles displayed strain-stiffening behavior due to nonaffine deformation of the bundle network. At low stress, the tensile load was carried by the cross-links and microtubule bending. At high stress, the bundle began to tighten toward its centerline and microtubule stretch became significant. Failure of axonal microtubule bundles was also investigated using dynamic simulations with critical strain criteria for the elastic elements. Catastrophic bundle failure was observed due to failure of cross-links. This resulted in pull-out of the microtubules, whereby cross-links failed and microtubules were able to slide past one another leading to bundle elongation and weakening. This effect may explain experimentally

observed axonal elongation and undulations following traumatic stretch injury. Microtubule rupture was not evident in dynamic simulations.

Previous studies have indicated that mechanical tension facilitates growth of the axon; this may well be associated with tensile loading of the microtubule bundle and subsequent growth. A combined mechanical and biochemical study of normal physiological and traumatic loading, as well as the downstream effects of such loading, would be particularly useful for studying axonal growth, mechanical stability, and injury. Furthermore, the mechanical properties of tau protein cross-links should be accurately described due to their suggested mechanical importance as evidenced by this study. Using computational and experimental techniques in symphony, it will indeed be possible to form a better understanding of the mechanical and biochemical behavior of axons under tensile loading.

APPENDIX: SENSITIVITY ANALYSIS

Sensitivity analysis was performed by varying the microtubule bending stiffness, microtubule elastic modulus, cross-link elastic modulus, and cross-link length. These parameter values were increased and decreased by 5%, 10%, and 50%. Simulations were performed with an average cross-link spacing of 50 nm and a tensile stress of 1 MPa, meant to represent intermediate simulation conditions. The resulting percent changes in the steady-state strain, percentage of energy stored in microtubule bending, percentage of microtubule stretching, and percentage of cross-link stretching were calculated (Fig. 9). It is evident that the model is not very sensitive to modest changes in the system parameters. This suggests that the model is applicable and the results are acceptable given parameter estimates with reasonable agreement to true physiological values.

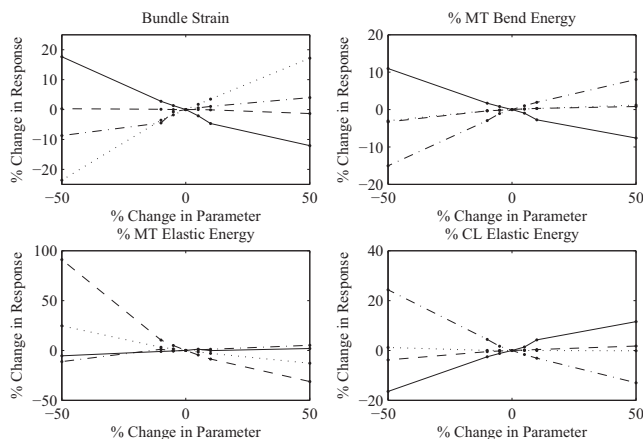


FIGURE 9 Sensitivity plots of the steady-state bundle response to system parameters. System parameters that are varied include microtubule bending stiffness (*solid line*), microtubule elastic modulus (*dashed line*), cross-link elastic modulus (*dash dotted line*), and cross-link length (*dotted line*). Response sensitivity is monitored for percent change in bundle strain (*top left*), percentage of energy stored in microtubule bending (*top right*), percentage of energy stored in microtubule stretching (*bottom left*), and percentage of energy stored in cross-link stretching (*bottom right*). The model shows relatively low sensitivity to modest changes in system parameters, lending confidence to the conclusions.

SUPPORTING MATERIAL

A table is available at [http://www.biophysj.org/biophysj/supplemental/S0006-3495\(11\)05452-X](http://www.biophysj.org/biophysj/supplemental/S0006-3495(11)05452-X).

The authors thank M. Azimi, R. Karimi, R. Moussavi-Baygi and Y. Jamali and the rest of Molecular Cell Biomechanics Laboratory for their assistance throughout the project, as well as S. Berger for his many helpful discussions and support.

REFERENCES

- Goldstein, L. S. B., and Z. H. Yang. 2000. Microtubule-based transport systems in neurons: the roles of kinesins and dyneins. *Annu. Rev. Neurosci.* 23:39–71.
- Guzik, B. W., and L. S. Goldstein. 2004. Microtubule-dependent transport in neurons: steps towards an understanding of regulation, function and dysfunction. *Curr. Opin. Cell Biol.* 16:443–450.
- Fadić, R., J. Vergara, and J. Alvarez. 1985. Microtubules and caliber of central and peripheral processes of sensory axons. *J. Comp. Neurol.* 236:258–264.
- Yu, W. Q., and P. W. Baas. 1994. Changes in microtubule number and length during axon differentiation. *J. Neurosci.* 14:2818–2829.
- Conde, C., and A. Cáceres. 2009. Microtubule assembly, organization and dynamics in axons and dendrites. *Nat. Rev. Neurosci.* 10:319–332.
- Coleman, M. 2005. Axon degeneration mechanisms: commonality amid diversity. *Nat. Rev. Neurosci.* 6:889–898.
- Becker, J. S., and M. Przybylski. 2007. Studies of structure and phosphorylation of tau protein using high resolution mass spectrometry. *J. Anal. At. Spectrom.* 22:761–765.
- Mandelkow, E., Y. H. Song, ..., E. M. Mandelkow. 1995. On the structure of microtubules, tau, and paired helical filaments. *Neurobiol. Aging.* 16:347–354.
- Rosenberg, K. J., J. L. Ross, ..., J. Israelachvili. 2008. Complementary dimerization of microtubule-associated tau protein: implications for microtubule bundling and tau-mediated pathogenesis. *Proc. Natl. Acad. Sci. USA.* 105:7445–7450.
- Chen, J., Y. Kanai, ..., N. Hirokawa. 1992. Projection domains of MAP2 and tau determine spacings between microtubules in dendrites and axons. *Nature.* 360:674–677.
- Park, E., J. D. Bell, and A. J. Baker. 2008. Traumatic brain injury: can the consequences be stopped? *CMAJ.* 178:1163–1170.
- Center for Disease Control and Prevention. 2010. Traumatic Brain Injury In The United States. CDC and U.S. Department of Health and Human Services, Atlanta, GA.
- Ertürk, A., F. Hellal, ..., F. Bradke. 2007. Disorganized microtubules underlie the formation of retraction bulbs and the failure of axonal regeneration. *J. Neurosci.* 27:9169–9180.
- Gaetz, M. 2004. The neurophysiology of brain injury. *Clin. Neurophysiol.* 115:4–18.
- Tang-Schomer, M. D., A. R. Patel, ..., D. H. Smith. 2010. Mechanical breaking of microtubules in axons during dynamic stretch injury underlies delayed elasticity, microtubule disassembly, and axon degeneration. *FASEB J.* 24:1401–1410.
- Janmey, P. A., U. Euteneuer, ..., M. Schliwa. 1991. Viscoelastic properties of vimentin compared with other filamentous biopolymer networks. *J. Cell Biol.* 113:155–160.
- Brangwynne, C. P., F. C. MacKintosh, ..., D. A. Weitz. 2006. Microtubules can bear enhanced compressive loads in living cells because of lateral reinforcement. *J. Cell Biol.* 173:733–741.
- Chandran, P. L., and M. R. K. Mofrad. 2009. Rods-on-string idealization captures semiflexible filament dynamics. *Phys. Rev. E.* 79:011906.
- Mofrad, M. R. K. 2009. Rheology of the cytoskeleton. *Annu. Rev. Fluid Mech.* 41:433–453.

20. Kim, T., W. Hwang, ..., 2009. Computational analysis of a cross-linked actin-like network. *Exp. Mech.* 49:91–104.
21. Silber, J., J. Cotton, ..., W. Grant. 2004. Computational models of hair cell bundle mechanics: III. 3-D utricular bundles. *Hear. Res.* 197:112–130.
22. Claessens, M. M. A. E., M. Bathe, ..., A. R. Bausch. 2006. Actin-binding proteins sensitively mediate F-actin bundle stiffness. *Nat. Mater.* 5:748–753.
23. Head, D. A., A. J. Levine, and F. C. MacKintosh. 2003. Deformation of cross-linked semiflexible polymer networks. *Phys. Rev. Lett.* 91:108102.
24. Onck, P. R., T. Koeman, ..., E. van der Giessen. 2005. Alternative explanation of stiffening in cross-linked semiflexible networks. *Phys. Rev. Lett.* 95:178102.
25. Tolomeo, J. A., and M. C. Holley. 1997. Mechanics of microtubule bundles in pillar cells from the inner ear. *Biophys. J.* 73:2241–2247.
26. Bathe, M., C. Heussinger, ..., E. Frey. 2008. Cytoskeletal bundle mechanics. *Biophys. J.* 94:2955–2964.
27. Sandersius, S. A., and T. J. Newman. 2008. Modeling cell rheology with the Subcellular Element Model. *Phys. Biol.* 5:015002.
28. Bertaud, J., Z. Qin, and M. J. Buehler. 2010. Intermediate filament-deficient cells are mechanically softer at large deformation: a multi-scale simulation study. *Acta Biomater.* 6:2457–2466.
29. Rodney, D., M. Fivel, and R. Dendievel. 2005. Discrete modeling of the mechanics of entangled materials. *Phys. Rev. Lett.* 95:108004.
30. Blundell, J. R., and E. M. Terentjev. 2009. Stretching semiflexible filaments and their networks. *Macromolecules.* 42:5388–5394.
31. Pampaloni, F., G. Lattanzi, ..., E. L. Florin. 2006. Thermal fluctuations of grafted microtubules provide evidence of a length-dependent persistence length. *Proc. Natl. Acad. Sci. USA.* 103:10248–10253.
32. Lele, T. P., and S. Kumar. 2007. Brushes, cables, and anchors: recent insights into multiscale assembly and mechanics of cellular structural networks. *Cell Biochem. Biophys.* 47:348–360.
33. Baas, P. W., C. Vidya Nadar, and K. A. Myers. 2006. Axonal transport of microtubules: the long and short of it. *Traffic.* 7:490–498.
34. Mehrbod, M., and M. R. K. Mofrad. 2011. On the significance of microtubule flexural behavior in cytoskeletal mechanics. *PLoS One.* 6:e25627.